JOURNAL OF PROPULSION AND POWER
Vol. 24, No. 5, September–October 2008

Hybrid Particle-in-Cell Erosion Modeling of Two Hall Thrusters

Shannon Y. Cheng* and Manuel Martinez-Sanchez†
Massachusetts Institute of Technology, Cambridge, Massachusetts 02139

DOI: 10.2514/1.36179

An axisymmetric hybrid particle-in-cell model of the Hall thruster plasma discharge has been upgraded to simulate the erosion of the thruster acceleration channel, the degradation of which is the main life-limiting factor of the propulsion system. Evolution of the thruster geometry as a result of material removal due to sputtering is modeled by calculating wall erosion rates, stepping the grid boundary by a chosen time step and altering the computational mesh between simulation runs. The code is first tuned to predict the nose cone erosion of a 200-W Busek Hall thruster, the BHT-200. Simulated erosion profiles from the first 500 h of operation compare favorably with experimental data. The thruster is then subjected to a virtual life test that predicts a lifetime of 1330 h, well within the empirically determined range of 1287–1519 h. The model is then applied to the BHT-600, a higher-power thruster, to reproduce wear of its exit ring configuration over 932 h of firing. Though some optimized code features remain the same, others need adjustment to achieve comparable erosion results. Better understanding of the physics of anomalous plasma transport and low-energy sputtering are identified as the most pressing needs for improved lifetime models.

I. Introduction

HALL thrusters are used for propulsion tasks such as geosynchronous orbit stationkeeping and other low-thrust orbit-adjusting maneuvers. These missions have primarily employed the thruster at a single nominal operating point and require electric propulsion lifetimes of 2000–3000 h [1], which is easily satisfied by thrusters like the SPT-100 with a 7000-h lifetime. As confidence in the technology builds, mission planners are investigating the feasibility of expanding the use of Hall thrusters to purposes ranging from interplanetary cargo transfer [2,3] to aerobraking [4]. To succeed at these functions, it may be desirable to throttle the thruster over a range of operating conditions, varying either power or specific impulse. The effect of this offnominal firing on the device's longevity has not been fully characterized, although a mechanism's expected lifetime is an important design metric that determines the number of thrusters needed for an extended cargo mission or whether the system is a cost-effective propulsion alternative for cost-capped science missions. Oftentimes, life testing done to qualify thrusters focuses on operating at full power to maximize propellant throughput in the shortest amount of time possible. However, during the actual mission, this full-power mode may not be the primary firing condition and lifetimes could be significantly longer than those predicted by experiment [5]. Clearly, it would be prohibitively expensive and time consuming to experimentally determine the life span of a thruster at every possible operating condition. Thus, the ability to accurately simulate the mechanisms that lead to failure of the thruster as well as how they are affected by differing firing regimes is required from a mission planning standpoint. Another benefit of a computational model for Hall thruster lifetime and erosion mechanisms is its contribution to the design process. Thruster designers need a tool to foresee how changes in their blueprints affect lifetime without running a costly life test after each design iteration. Having a predictive capability expedites the process by allowing only promising concepts to reach the materialized phase. In addition, once a finalized design is established, the simulation can be used to aid in thruster qualification by performing a virtual life test.

Received 17 December 2007; accepted for publication 31 March 2008.

*Research Assistant, Department of Aeronautics and Astronautics, 77 Massachusetts Avenue. Student Member AIAA.

†Professor, Department of Aeronautics and Astronautics, 77 Massachusetts Avenue. Senior Member AIAA.

II. Lifetime Definition

The lifetime of a Hall thruster is mainly limited by the erosion of components protecting its magnetic circuitry from the discharge plasma. Once the magnetic poles are exposed, further degradation or overheating may occur, affecting the nominal magnetic field and consequently the thruster's performance. Accordingly, end of life is declared when the ceramic exit rings in stationary plasma thrusters (SPT) or the metal guard rings in thrusters with anode layer (TAL) are breached. These two Hall thruster variants and their sensitive components are illustrated in Figs. 1 and 2.

III. Prior Work

A. Experimental Work

Experiments related to thruster longevity primarily fall into two categories. Long-duration qualification tests aim to directly determine lifetime by operating the thruster for lengthy periods in a continuous fashion [6–14]. Results differ between thrusters, but tests have proven lifetimes on the order of thousands of hours and show that, though performance parameters (thrust, efficiency, and specific impulse) may exhibit some variation at the beginning of life, values do not deviate greatly from nominal and tend to stabilize later in life. Asymmetric erosion around the acceleration channel is also commonly observed, but the cause for this azimuthal variation is not well understood.

In addition to these lengthy tests, shorter experiments have also been performed with the aim of characterizing erosion behavior to allow for extrapolation of lifetime. Trials using five different grades of boron nitride (BN) exit rings in the laboratory model NASA-120M Hall thruster show significant variation in erosion profiles after 200 h [15]. Testing of a D-80 in different operating modes for 100 h proves that erosion is highly dependent on firing conditions and exhibits a nonlinear relationship between erosion rate and applied voltage [16]. Spectroscopy has also been used to quantify overall erosion rates with a nonintrusive method that does not require interruption of the life test to physically measure a wear profile [17–20]. In these experiments, the intensity of emission lines from sputtered wall material is used to determine the rate and confirms that erosion depends on operating conditions. Finally, the influence of magnetic field topology on the initial upstream location of channel wear is used in conjunction with a numerically simulated wall energy distribution to estimate the sputter threshold of the thruster ceramic [21].

Though these results provide much insight into the issue of lifetime prediction, they also indicate the problem is complex, not only being thruster-dependent, but also specific to wall material and operating condition.

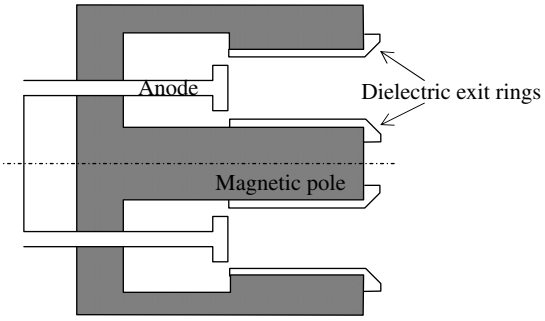

Fig. 1 Stationary plasma thruster (SPT).

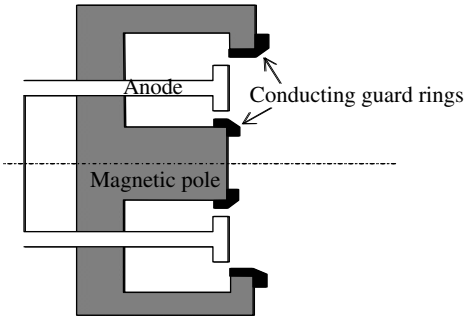

Fig. 2 Thruster with anode layer (TAL).

B. Lifetime Prediction Models

Besides work done to empirically quantify lifetime and erosion mechanisms of Hall thrusters, development of predictive lifetime models has also been pursued. The basis of all these models gives the wall recession rate ξ as

$$\xi = j_{iw} S_v(E_i, \theta_i) \tag{1}$$

where j_{iw} is the ion flux to the wall and $S_v(E_i, \theta_i)$ is the volumetric sputtering coefficient that is a function of the target material, the incident ion energy E_i, and the ion angle of incidence θ_i. Thus, necessary components of any life span forecasting tool are a sputter model for the material in question and a plasma discharge model that gives the wall flux. Though both theoretical and semi-empirical models have been developed to predict Hall thruster lifetime, this summary will focus on reviewing existing computational models.

A number of approaches to numerically simulating the erosion processes in a Hall thruster and their consequences on lifetime have recently emerged. In 2004, Manzella et al. [22] proposed a lifetime prediction model that attributed the mechanism for wall erosion to scattering collisions, arguing that ions impacting the wall must have been diverted from an otherwise uniform plasma flow along the acceleration channel. Building a 1-D model around this theory, decent agreement to erosion profiles of the SPT-100 is achieved, but only when the neutral density is increased by a factor of two. Because scattering collisions alone do not produce enough erosion, the assumption of an ideally-focused axial flow is improbable.

Continuing work on this issue, Yim et al. [23–25] have expanded on these ideas and developed a 2-D fluid model more grounded in physics. The hydrodynamic description models the plasma species with a finite volume flux-splitting method on an axisymmetric Cartesian mesh. To allow for a changing geometry as the walls erode, a cut cell method is used. In addition to a model for the sputter yield, near-wall scattering collisions are included, ion wall fluxes are given a Maxwellian distribution, and the Bohm coefficient is varied to affect the potential profile across the channel. Simulation results tend to underpredict erosion at long times and is weakest at capturing the upstream erosion behavior.

The remaining computational modeling has focused on using 2-D hybrid particle-in-cell (PIC) codes to provide the plasma discharge parameters. In a study to determine the effect of different magnetic field configurations on the SPT-100, Garrigues et al. [26] included a sputtering model to analyze the influence on lifetime. The main conclusion of the analysis confirms the fact that erosion damage to thruster walls decreases when more of the plasma's potential drop occurs outside the channel. This result is already well understood in the context of TALs that exhibit less erosion than their SPT counterparts due to the acceleration zone being pushed outside the thruster.

An existing code, HPHall [27,28] has been built upon by Gamero-Castaño and Katz [29] as the foundation of their lifetime prediction capability. Over the course of a simulation run, averaged flux and energy distributions to the channel walls are tracked. During postprocessing, these properties are used to generate sputter yields and then erosion rates. Armed with these, the geometry is stepped forward in time and the process is repeated, allowing self-consistent modeling of the geometry evolution. The SPT-100 is used as the test case because erosion profiles over its lifetime are available for direct comparison in the literature [30]. Computational efforts yield results that correctly place the location of channel erosion onset, but overall erosion is underpredicted. Further work on the model is being done to improve neutral injection, wall sheath, and electron mobility modeling with the intent of better matching erosion data [31,32].

Sommier et al. use a simulation modeled after HPHall as its research base [33,34]. Instead of postprocessing with averaged properties, sputtering caused by individual particles crossing the grid boundary is tracked. Neutral sputtering is accounted for, but found to be a factor of 1000 less than that caused by ions. Both charge exchange (CEX) and momentum exchange ion-neutral collisions are modeled; CEX tends to decrease whereas momentum exchange collisions increase erosion. Overall, erosion is decreased by these interactions. The effect of self-induced magnetic fields is also found to have a minimal effect on the simulation results. Both the Stanford Hall Thruster and SPT-100 are subjected to a virtual life test with the model. Erosion profile data for the Stanford Hall Thruster are unavailable, and so only comparison with the SPT-100 profiles gives an indication to the success of the code. As with Gamero's model, Sommier's findings underpredict erosion.

C. Discussion of Previous Work

Based on the experimental work that has been done in this area, the need for prediction tools is apparent. Full lifetime tests are expensive, time-consuming, and do not cover the entire range of possible operating conditions. Nevertheless, empirical data are crucial for validating proposed models and should be continued. Theoretical models provide a general and simple picture of the erosion issue, but are unlikely to give detailed insight into the thruster-specific problem. Semi-empirical accelerated wear tests attempt to address these concerns but still involve destruction of a thruster, which may not be desirable in early design stages or if cost is a consideration.

Thus, simulations have the greatest potential to provide a resource-efficient solution as a good model should be able to handle a variety of thruster configurations at different operating conditions. Upon reviewing the current numerical work being done, the greatest roadblock seems to be difficulty in acquiring a complete set of key information needed for successful lifetime modeling. Thruster geometry is usually not a problem, whereas magnetic field configuration is more difficult as these designs are generally proprietary. To model the SPT-100, Gamero and Sommier both used a combination of experimental centerline measurements of the field and a magnetic streamline map from Garrigues that represented the typical configuration. When regridding to account for erosion of the walls, assumptions had to be made about the field in the newly exposed regions. As the magnetic field plays a fundamental role in Hall thruster plasma dynamics, it is difficult to expect good results if this input is suspect in any way. Another complication is a lack of understanding of material sputtering behavior at low energy. All the computational models discussed use the same experimental sputter yield data of borosil, the SPT-100 channel ceramic, taken by Garnier [35]. However, the data points are taken at higher energies than those typically seen in a Hall thruster and a method for approximating

Table 1 Comparison of borosil sputter thresholds used in computational models

Model	E_{th}, eV	Reference
Manzella	50	[22]
Yim	50	[23]
	70	[24]
	50, 60, 70	[25]
Garrigues	30–70	[26]
Gamero	56.9	[29]
Sommier	50	[33,34]

sputter behavior at low energies is necessary. The approaches taken by the modelers range from logarithmic curve fits to using the form of a theoretical model developed for elemental sputtering. These disparities are further highlighted by an inability to converge on the sputter threshold value E_{th} the fundamental parameter of these models. Table 1 illustrates the differences across and sometimes within simulations.

The development of the model in this paper strives to overcome these obstacles by being as detailed as possible in the definition of thruster-specific parameters. Also, when faced with uncertainty in the physics, an effort is made to base the applied solution on solid theory. Two low-power thrusters developed by Busek Co., the BHT-200 and the BHT-600, are studied. These thrusters are chosen because a complete set of data needed for lifetime prediction can be compiled. Geometry and magnetic field information are acquired from Busek Co., sputtering data on the identical grade of channel ceramic have been taken, and erosion profiles for simulation comparison are also accessible. Once the model is tuned for one thruster, its applicability to the other thruster is tested to determine if all appropriate physics affecting erosion has been implemented.

IV. Sputter Model

To quantify the degradation of Hall thruster lifetime due to erosion of the acceleration channel by the plasma flow, a sputter yield model for the channel material is required. In this paper, the two thrusters considered both have BN lining their acceleration channels. BN is an attractive choice for insulation of the magnet poles due to its mechanical strength and thermal shock resistance. In comparison with other insulator materials, BN also exhibits lower erosion rates.

A. Normal Yield Model

Because available experimental data on BN sputter yields do not address the low-energy regime, where the majority of ions in a Hall thruster fall, the approach is to use an analytical model and rely on experimental data for calibration. It has been seen experimentally that different grades of BN have different sputter properties. As such, in developing the sputter yield model, only data taken by Yalin et al. [36] are used because the BN grade experimented on is identical to that used in construction of both the BHT-200 and the BHT-600. The model adapted for use is that of Yamamura and Tawara [37] who give a theory-based analytical formula that has been empirically tested against available data and is valid for any ion–target combination, though only monatomic targets are included. Following the outlined procedure, the normal sputter yields for boron and nitrogen are calculated and presented in Fig. 3. For comparison, Yalin's data as well as the average of the Yamamura and Tawara-predicted B and N yields are also plotted. Although the analytical formula underpredicts the experimental sputter yield, the results are on the same order of magnitude and show reasonable agreement considering the formula is calibrated to monatomic solids.

The form of Yamamura and Tawara's formula for normal sputter yield Y_n is

$$Y_n(E) = 0.042 \frac{Q(Z_2)\alpha^*(M_2/M_1)}{U_s} \frac{S_n(E)}{1+\Gamma k_e \epsilon^{0.3}} \left[1 - \sqrt{\frac{E_{th}}{E}}\right]^{2.5} \quad (2)$$

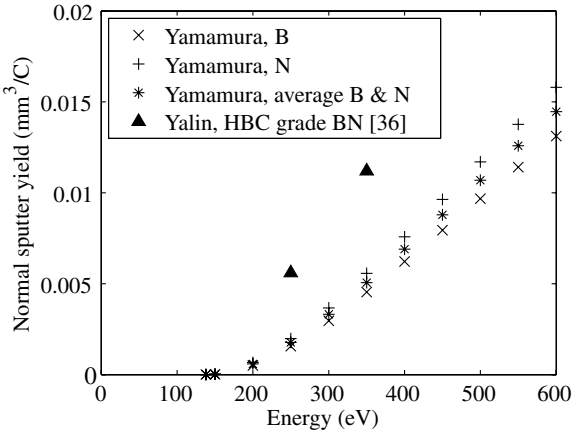

Fig. 3 Comparison of $Xe^+ \rightarrow$ BN analytical and experimental normal sputter yields.

where E is the energy in electron volts; E_{th} is the threshold energy in electron volts; $Q(Z_2)$, $\alpha^*(M_2/M_1)$, U_s, Γ, and k_e are constants of the projectile–target combination; ϵ is the reduced energy and is linear in E for a given projectile–target combination; and $S_n(E)$ has an energy dependence defined by an analytical expression based on the Thomas–Fermi potential, s_n^{TF}:

$$s_n^{TF}(\epsilon) = \frac{3.441\sqrt{\epsilon}\,\ell n(\epsilon + 2.718)}{1 + 6.355\sqrt{\epsilon} + \epsilon(6.882\sqrt{\epsilon} - 1.708)} \quad (3)$$

Because the constants determined by the projectile–target combination are not known for the BN ceramic, it is desirable to find a fit that incorporates parameters that represent these unknowns. For small values of ϵ, Eq. (3) scales $\sim\sqrt{\epsilon}$. Thus, a fit of the form

$$Y_n(E) = \frac{AE^{0.5}}{1 + BE^{0.3}} \left(1 - \sqrt{\frac{E_{th}}{E}}\right)^{2.5} \quad (4)$$

is proposed, where A and B are fitting parameters. To test its validity, the approximation is compared with the full expression for boron and nitrogen, because all parameters needed to evaluate Eq. (2) are known. These comparisons are given in Figs. 4 and 5, only the range of low energies relevant to the problem is considered. It is apparent that the fit as given in Eq. (4) does not agree well with the Yamamura model curve because the energy dependence of Eq. (3) is not adequately captured. However, if the fit exponent is changed to a value of 0.474, excellent matching is achieved for both elements. Thus, the revised fit

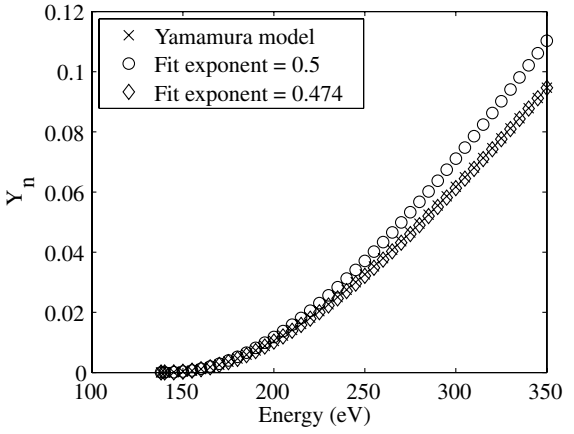

Fig. 4 Comparison of Yamamura model to Eqs. (4) and (5), boron.

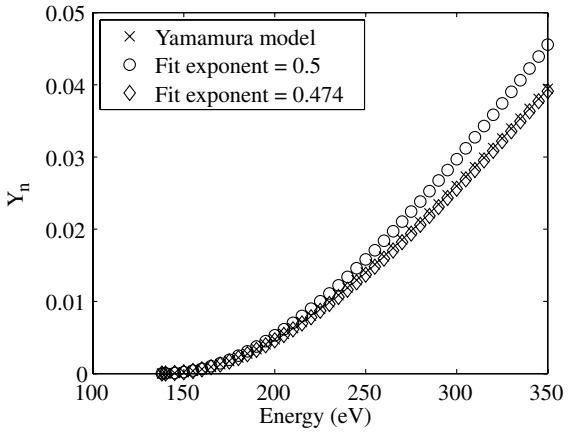

Fig. 5 Comparison of Yamamura model to Eqs. (4) and (5), nitrogen.

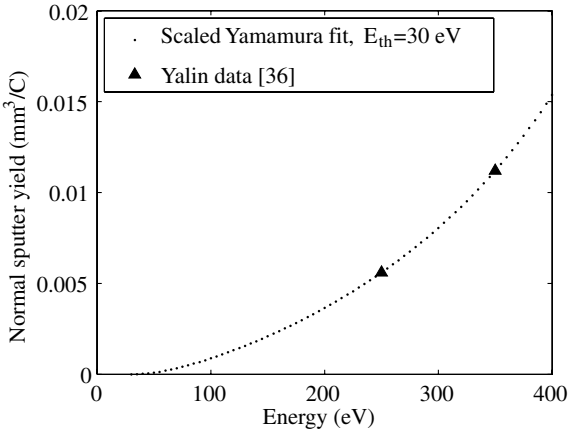

Fig. 6 Yield fit for $E_{\text{th}} = 30$ eV.

$$Y_n(E) = \frac{AE^{0.474}}{1 + BE^{0.3}}\left(1 - \sqrt{\frac{E_{\text{th}}}{E}}\right)^{2.5} \tag{5}$$

is used.

Using Yalin's BN data, best-fit values of A and B are found for several energy thresholds. These values are given in Table 2. Figure 6 plots the yield fit corresponding to a 30 eV energy threshold and Fig. 7 shows the fits for a range of threshold energies in the near-threshold region. All of these curves pass through Yalin's experimental data points at higher energies. It is apparent that selection of E_{th} is quite important as it can shift the yield curve a significant amount. Because the threshold energy of BN is not known, choice of the appropriate E_{th} is one of the goals of the modeling.

B. Angular Yield Model

The angular dependence of the sputter yield is also based on a Yamamura empirical formula [38]. For the case of heavy-ion sputtering, the angular yield Y_θ has the form

$$Y_\theta(Y_n, E, \theta_i) = Y_n \times \cos^{-F}(\theta_i) \times e^G \tag{6}$$

where Y_n is the normal yield, E is the incident energy in electron volts, θ_i is the incident angle, and F and G are given by

$$F = -f\left(1 + 2.5\frac{aE^{-1/2}}{1 - aE^{-1/2}}\right), \qquad G = -\Sigma\left(\frac{1}{\cos(\theta_i)} - 1\right)$$

where $f = 5.97563$, $a = -3.63786$, and $\Sigma = 1.41355$. Figures 8 and 9 show the angular yield fits plotted against the experimental data for 250 and 350 eV.

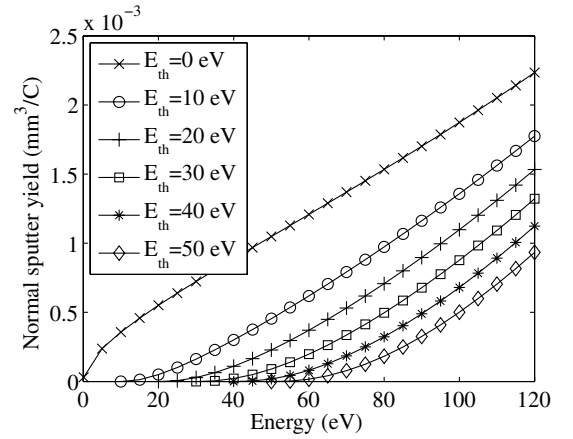

Fig. 7 Near-threshold region yield fits.

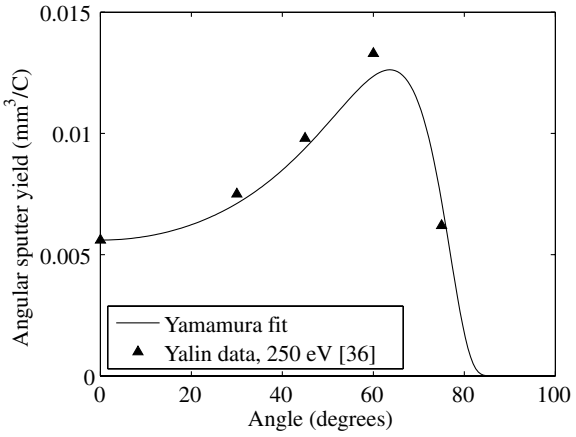

Fig. 8 Yamamura-based angular sputter yield model, 250 eV.

V. Plasma Model

The model of the plasma discharge is based on HPHall [27,28], an existing well-proven Hall thruster simulation. HPHall is an axisymmetric model of the area between the anode and cathode. The primary inputs are a 2-D mesh of the simulation region as well as the thruster's magnetic field. Because induced magnetic fields are ignored, this **B** field is considered static. In a balance between detailed physics and heavy computational burden, a hybrid PIC approach is taken; namely, the heavy-ion and neutral species are modeled as discrete particles whereas the light electrons are represented as a fluid. An assumption of quasi neutrality, $n_i = n_e$, links the ion and electron submodels through their densities and further reduces required effort by allowing grid spacings larger than the Debye length. Because the nonneutral wall sheaths are not resolved, an analytic model satisfying the Bohm condition is imposed at relevant grid boundaries to include their effect [39].

To better capture the evolving wall boundary, an overhaul of the particle mover to rigorously follow the heavy species is implemented

Table 2 Fitted parameters for $Xe^+ \rightarrow$ BN normal yield approximation

E_{th}, eV	A	B
0	0.0000835484	−0.151824
10	0.000164433	−0.146887
20	0.000233999	−0.143251
30	0.000320828	−0.139106
40	0.000436831	−0.133966
50	0.000600157	−0.12718

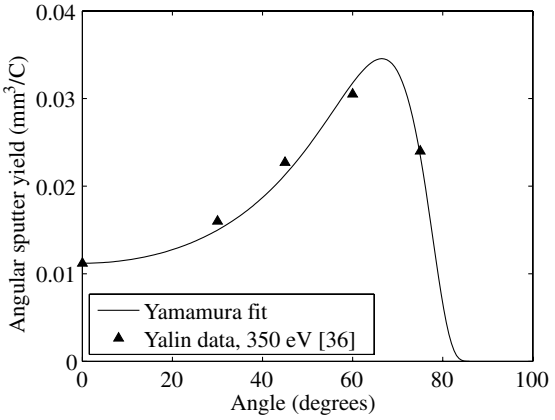

Fig. 9 Yamamura-based angular sputter yield model, 350 eV.

to allow accurate tracking of ions as they leave the simulation domain. Individual ions that cross the grid boundary where ceramic is located cause sputtering and contribute to the thruster's erosion. Using the particle's incident energy and angles, which are determined by the ion velocity, the plasma potential, and the wall sheath, the volumetric amount of material sputtered is calculated using the model in the preceding section. This yield is then converted to an equivalent erosion depth, which is tracked at wall boundary nodes. After running the simulation for an appropriate amount of time, an erosion rate at each wall node can be calculated and the boundary is advanced forward in time to the next iteration. The geometry and corresponding magnetic field are recalculated and the procedure is repeated until the desired number of hours of operation have been achieved. Figure 10 shows the procedural flow chart for modeling the thruster erosion.

Anomalous transport is modeled in HPHall by including a constant term in the cross-field electron mobility to represent the greater-than-classical diffusion observed in Hall thrusters,

$$\mu_{e,\perp} = \frac{\mu_e}{\beta_e^2} + K_B \frac{1}{16B} \tag{7}$$

where $\mu_e = e/\nu_{\text{en}} m_e$ is the electron mobility, $\beta_e = \omega_c/\nu_{\text{en}}$ is the electron Hall parameter, and K_B is the Bohm coefficient. K_B is a parameter adjustable between 0 and 1 and is used to tune the code. However, experimental evidence shows that the anomalous electron mobility is highly correlated with the $E \times B$ drift velocity shear, giving rise to a transport barrier near the exit channel of the thruster [40]. The exact definition of the physics describing this behavior is a topic still under investigation [41,42], but is beyond the scope of this work to explore. Nevertheless, the effect exists and is important in determining the nature of the plasma discharge and subsequently its erosion of the channel walls. Thus, a method is implemented to manually impose a transport barrier in an educated manner, a technique that has been successful with other thruster models [43–45]. The imposed transport barrier is specified by prescribing a range of axial coordinates in which the anomalous Bohm diffusion is quenched or where only classical transport is applied. Outside of the barrier, the usual method of adding the constant Bohm coefficient to the classical contribution of the electron mobility is followed. The exact location and thickness of the barrier is thruster dependent and, without further information, requires tuning.

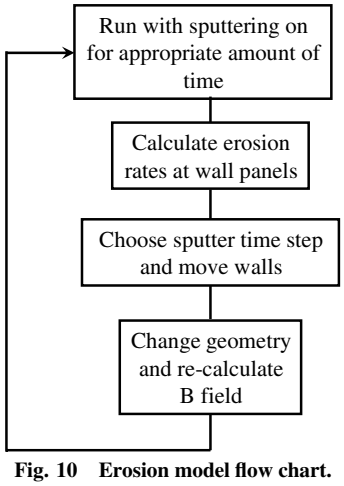

Fig. 10 Erosion model flow chart.

Table 3 BHT-200 nominal specifications

Discharge input power	200 W
Discharge voltage	250 V
Discharge current	0.8 A
Propellant mass flow rate	0.94 mg/s
Thrust	12.8 mN
Specific Impulse	1390 s
Propulsive efficiency	43.5%

VI. BHT-200 Modeling

The BHT-200, pictured in Fig. 11, is a low-power Hall thruster developed by Busek Co. Its nominal specifications are summarized in Table 3 [46]. A series of experimental nose cone profiles taken in 100-h increments during the first 500 h of thruster life are available for comparison with simulation results. An optical comparator, with an estimated error of ± 0.127 mm, was used to take the measurements.

The 53×22 computational mesh is based on the thruster geometry depicted in Fig. 12. The inner nose cone is made of HBC-grade BN and its erosion is the lifetime-limiting factor of the engine. Figure 13 shows a detailed view of the mesh near the nose cone, and an X marks

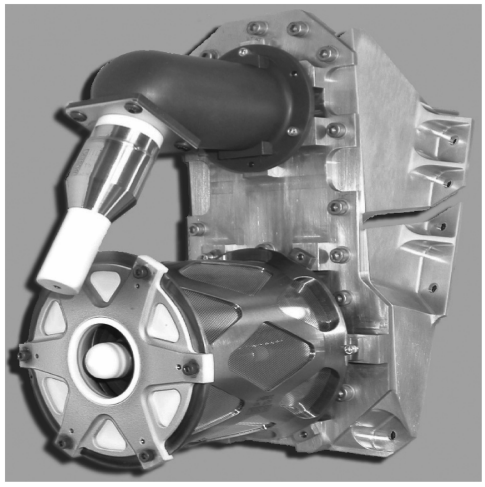

Fig. 11 BHT-200 thruster.

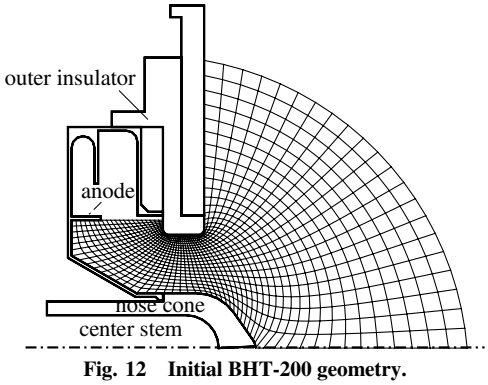

Fig. 12 Initial BHT-200 geometry.

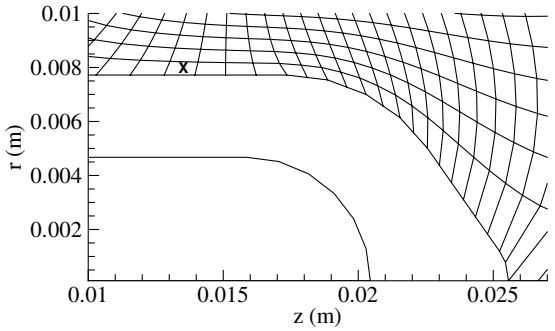

Fig. 13 Detail of BHT-200 nose cone panels.

the panel corresponding to the start of the BN material. This panel and those lying downstream are subject to sputtering according to Sec. IV's model and will move as the ceramic erodes. The magnetic field on this and subsequent grids is interpolated from the designed field.

Each simulated lifetime increment requires three HPHall runs. To fill the grid with neutrals, 20,000 iterations of neutrals-only mode are performed. Next, 1400 iterations in normal (all plasma species simulated) mode are used to bypass an initial transient the code exhibits before settling into steady thruster operation. Finally, a longer run in normal mode is done to establish a profile of wall erosion rates at this point in the thruster's life. For the BHT-200 geometry, these runs are performed for 20,000 iterations because this choice is a good compromise between reaching the steady-state erosion rates and having reasonable run times. All runs use an iteration time step of 5×10^{-8} s.

A. Parameter Tuning

A sputter time step of 100 h is chosen because the experimental wall profiles are advanced 100 h between lifetime runs. To test that 100 h is a reasonable increment to take, two cases are performed with identical input parameters. Figure 14 shows the wall profiles after 500 h of operation for the two cases. Case 1 takes steps of 100 h and represents the ending wall profile after five lifetime runs. Case 2 takes steps of 50 h and represents the final wall profile after 10 lifetime runs. The two cases are virtually identical, meaning 100-h time steps are reasonable.

Extensive tuning of the simulation to the erosion profiles from the first 500 h of operation is performed to determine model inputs. A sputter threshold of 30 eV is selected because it best corresponds to the overall level of erosion. In addition, inclusion of double ions has a significant effect on the wear profiles. Though only a small contribution to the ion flux, their higher energies give them much higher damage potential. The final parameters to be tuned relate to the anomalous transport model. The Bohm coefficient and location of the imposed transport barrier affect the positioning of the thruster plasma and, consequently, the erosion. It is found that a Bohm coefficient of 0.15 and an imposed transport barrier between $z =$ 0.015–0.0175 m give the best comparison. Further details on the tuning process can be found in [47].

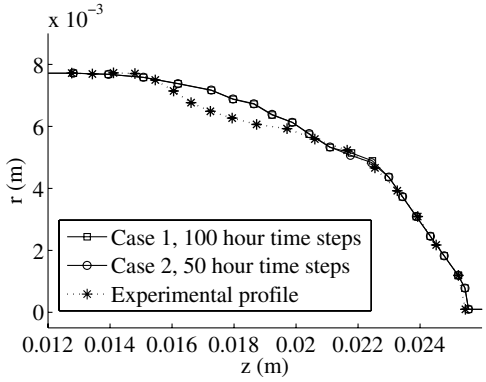

Fig. 14 BHT-200: comparison of sputter time steps at 500 h of operation.

B. Model Results

Using the tuned parameters, Fig. 15 shows the evolution of the wall profile. Erosion is generally well predicted, though the simulation begins to deviate from the experiment in the downstream region later in time. These input parameters are then used to run a simulated life test. Continuing from the accumulated 500 h of simulated operation, the thruster is stepped in 100-h increments until 900 cumulative hours are reached. Beyond 900 h, the time step between runs is selected on a case-by-case basis, but never exceeds 100 h. Time steps less than 100 h are chosen to allow smooth capture of the wall evolution (avoiding crossing of nodes); boundary nodes are redistributed as needed to maintain a constant number of evenly-spaced wall panels. In total, 15 runs are carried out, and the thruster first breaks through to the center stem at a time of 1330 h and at an axial location of $z \sim 0.01825$ m. Figure 15f shows the end of life profile. The simulated discharge current is 0.707 A and simulated thrust is 10.934 mN.

The BHT-200 that underwent 500 h of experimental life testing at Busek was subsequently sent to the U.S. Air Force Research Laboratory at Edwards Air Force Base for completion of the long-duration test. In total, the thruster was run for over 1700 h before the test was voluntarily terminated. Unfortunately, the experiment was not interrupted to take erosion profiles at intermediate times, and there are no further data to compare with. However, visual observations made of the nose cone tip falling off bracketed the insulator breach falling off between 1287 and 1519 h of thruster firing, putting the simulated lifetime of 1330 h in the correct range.

VII. BHT-600 Modeling

The BHT-600 is another member of the low-power Hall thruster family developed at Busek Co. and is pictured in Fig. 16. Its nominal specifications are summarized in Table 4 [46]. Being larger in size, the BHT-600 forgoes a nose cone in favor of the more traditional exit ring configuration. Wall erosion profiles taken during life testing at Edwards Air Force Base are available for tuning of the code. Experimental profiles were taken using optical profilometry at 80, 225, 368, 494, 665, and 932 h of thruster operation.

The 63×27 computational mesh is based on the thruster geometry depicted in Fig. 17. Both the inner and outer exit rings are made of HBC-grade BN, the same ceramic used for the BHT-200 nose cone. The BHT-600 thruster used for the life test arrived at Edwards having already been operated for 80 h. During this initial period, a variety of operating conditions were used as well as the cathode being moved further from the discharge chamber. All these changes undoubtedly have an effect on the erosion. Accordingly, as shown in Fig. 18, the baseline mesh is based instead on the 80-h erosion profile because the thruster operating parameters were kept constant from this point on in the life test.

As before, each simulated lifetime increment requires three HPHall runs. The initial sequence is identical to that of the BHT-200, with 20,000 iterations of neutrals-only mode followed by 1400 iterations in normal mode. The long normal mode runs to establish wall erosion rates are performed for 10,000 iterations. Fewer iterations are required for the BHT-600 geometry because it is less complex than that of the BHT-200 and the steady-state erosion rates are reached sooner.

Based on experience with the BHT-200, a sputter threshold of 30 eV, inclusion of double ions, and sputter time steps less than 100 h are maintained. The anomalous transport model parameters are retuned to represent the different thruster. Best results are achieved for a Bohm coefficient of 0.20 and an imposed transport barrier between $z = 0.003$–0.0045 m. Figures 19 and 20 show results at 494 and 932 h of operation. The simulation tends to overpredict erosion ahead of the exit ring chamfer and underpredict along the chamfer. Results do capture the higher erosion rates observed on the inner insulator. The simulated discharge current is 1.975 A and the simulated thrust is 30.529 mN.

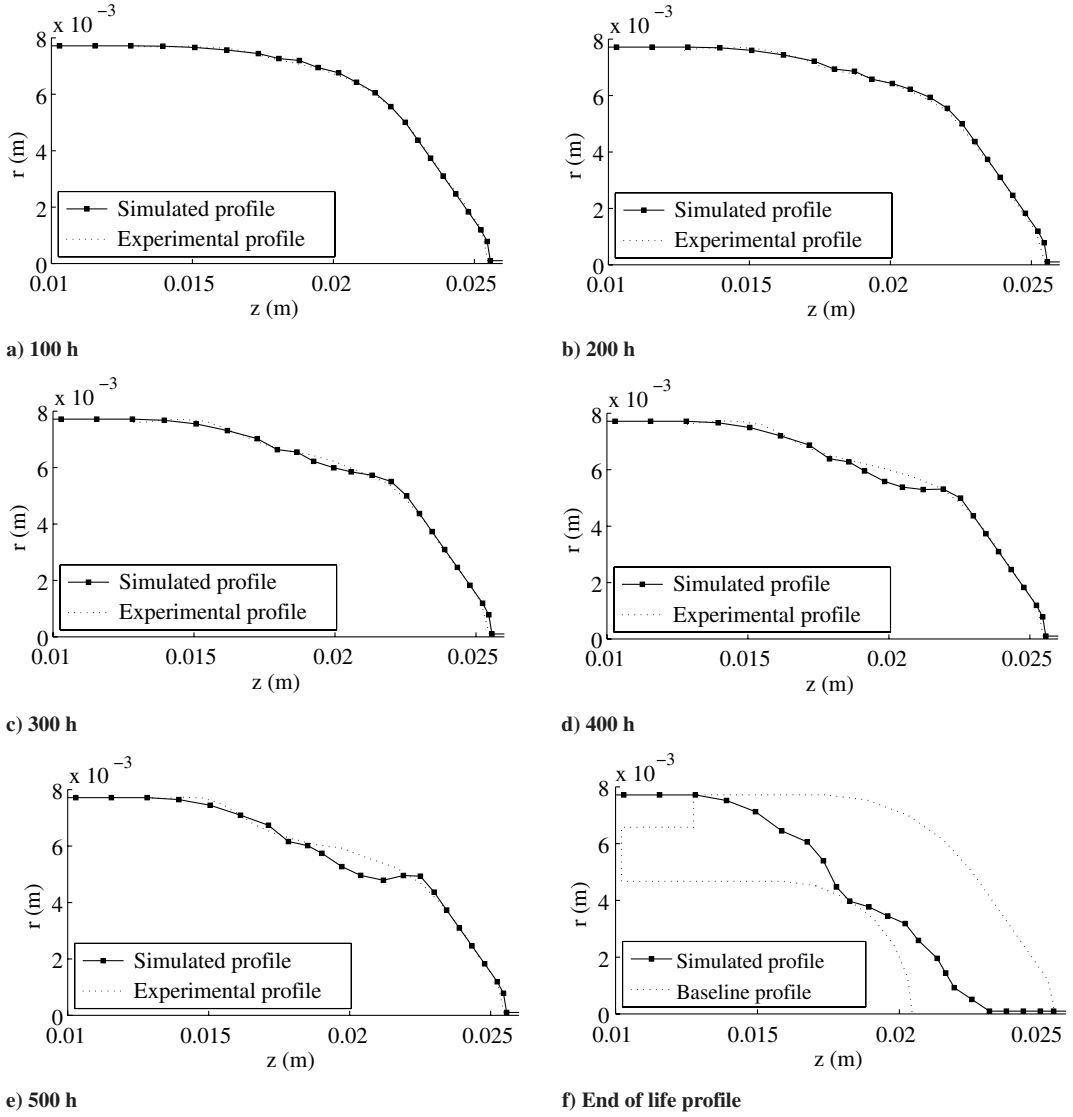

Fig. 15 BHT-200: erosion profile evolution.

VIII. Discussion

The problem of Hall thruster lifetime prediction has been addressed by developing a computational method and testing it against two thruster geometries with empirical data available for comparison. Though the model does not exactly reproduce experimental erosion profiles, it does provide wall regression rates of the right order throughout the thruster's lifetime. As a result, overall agreement of the channel evolution is achieved.

It is observed that the erosion behavior of the two thrusters studied is quite different. In the BHT-200, the majority of the wear occurs before the bending of the nose cone away from the channel centerline. The BHT-600, however, exhibits greatest erosion along the chamfer of its exit rings. Because of this disparity in the placement of the degradation, it is found that erosion rates in the two thrusters are affected by different factors. Figure 21 shows the 200-W thruster erosion rate at 500 h of operation whereas Figs. 22 and 23 are the flux and energy distributions. The erosion rate closely tracks the incident energies greater than about 100 eV. In the upstream section,

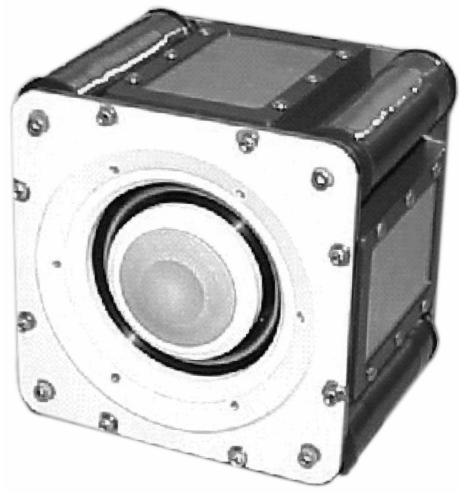

Fig. 16 BHT-600 thruster.

Table 4 BHT-600 nominal specifications

Discharge input power	600 W
Discharge voltage	300 V
Discharge current	2.05 A
Propellant mass flow rate	2.6 mg/s
Thrust	39.1 mN
Specific Impulse	1530 s
Propulsive efficiency	49.0%

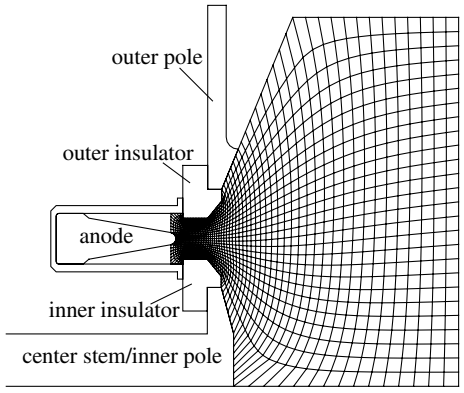

Fig. 17 BHT-600 geometry.

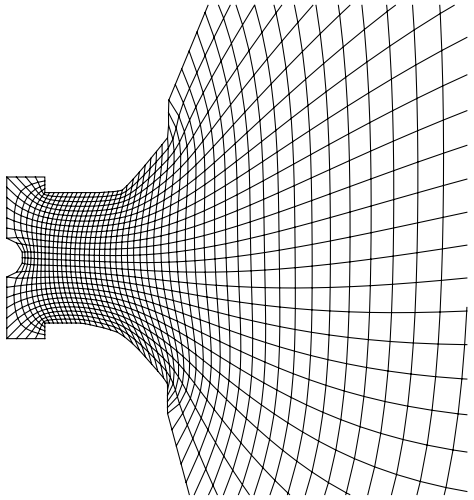

Fig. 18 BHT-600: detail of initial mesh after 80 h of operation.

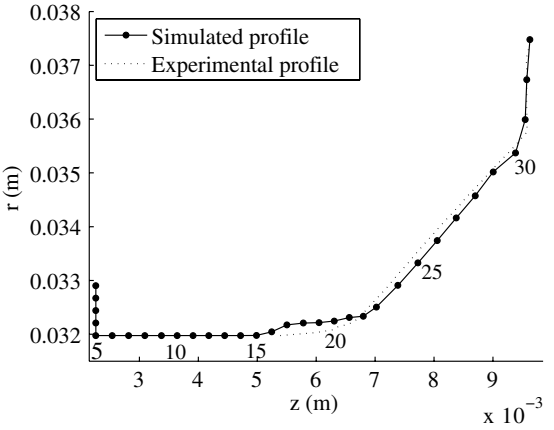

a) Outer insulator

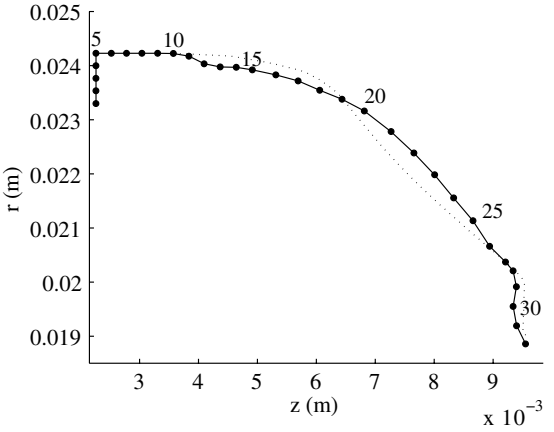

b) Inner insulator

Fig. 19 BHT-600: erosion profiles at 494 h.

the incident ions have approximately equal kinetic (from acceleration through the potential drop) and potential (from the fall through the wall sheath) contributions. As ions are accelerated further down the channel, the kinetic portion begins to dominate. In this thruster, because the number of impacting particles exceeds a certain threshold in the region of wear, flux is not a strong erosion indicator, except at the bend of the nose cone where a high impinging flux is associated with a peak in the erosion rate. Figure 24 shows little correlation between the ion incident angle and erosion; angles primarily between 30 and 40 deg are found in the region of greatest erosion, corresponding to the lower section of the sputtering curve.

Figures 25–27 show the same distributions along the inner insulator of the 600-W thruster at 494 h of operation. In this higher-power thruster, a relationship between the erosion rate and the other variables is not as easily seen. Because the bulk of the degradation happens in an area that is harder for the plasma to reach, the distribution of the wear rate is dictated by both the flux and the energy. For example, though node 15 is a local maximum on the energy distribution, it is a local minimum for the erosion rate. Upon examining the flux distribution, this location's resistance to wear is explained by a decreased influx. Again, the incident ion angle in Fig. 28 gives little indication of the erosion rate. Thus, until the physics of the thruster plasma and its location are better understood, device-specific tuning of the anomalous transport model is required to place the discharge correctly in a thruster. As the nature of the plasma changes between operating conditions of the same thruster, parameter selection also needs to occur for each case.

Double ions play an important role in the thruster erosion. Though they account for less than 10% of the wall flux, the addition of the BHT-200 increases erosion rates by a factor of 1.5–2. In the BHT-600, double ions are less than 5% of the wall flux but can increase erosion by a factor as high as 2–2.5. Because of this pronounced effect, double ions should be included in any lifetime prediction model.

As evidenced in the work with the BHT-200, it is possible to tune the simulation to a shorter test and then complete the life test numerically. The short-duration test should be long enough that a reasonable amount of wall material has been removed. For the BHT-200, 300 h is sufficient. When the same approach is applied to the BHT-600, reasonable agreement is achieved with the later profiles, but more work on the transport model is needed to correctly place the plasma in the discharge channel. Nevertheless, features observed during the early stages of the simulation are carried through the virtual lifetime test. Thus, matching of profiles early in life would lead to accurate predictions of those later in life. A cautionary note should be provided to those attempting to predict the terminal wall profile based on erosion rate measurements from the start of thruster life. Figure 29 compares projected wall profiles of the BHT-200 at 1330 h when erosion rates from 500 and 1270 h are used. The two projections give quite different views on the thruster state at this point. At 1330 h, the projection from 500 h has already broken through the nose cone to the center stem and the thruster end of life (EOL) would have been earlier. Furthermore, the location of the breach would have been further downstream. It can be seen that the time dependence of the erosion rates due to the gradual exposure of the nose cone tip to the plasma is not captured as it remains uneroded.

Despite the model's success at capturing erosion behavior, it is deficient at simultaneously reproducing performance parameters. Cases that agree better with nominal discharge current and thrust do not necessarily correlate with improved wear prediction. Hence, the matching of simulated and experimental bulk properties should not be the sole metric in calibrating thruster codes, as correctly capturing the detailed plasma distribution is not guaranteed. Because close attention is paid to the geometry and magnetic field definitions, this

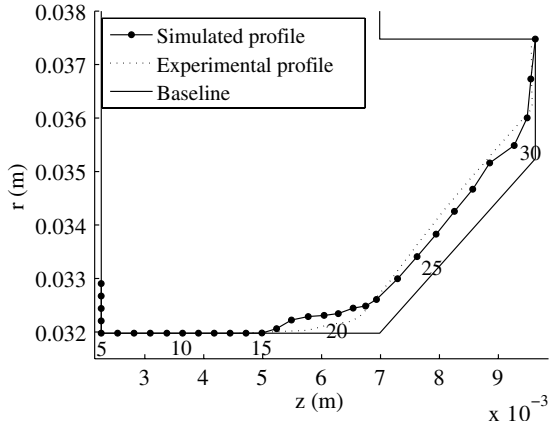

a) Outer insulator

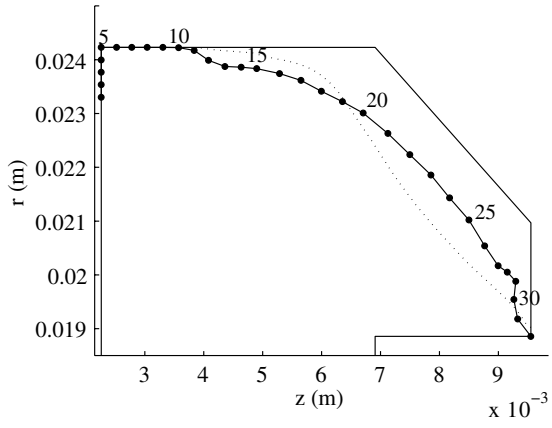

b) Inner insulator

Fig. 20 BHT-600: erosion profiles at 932 h.

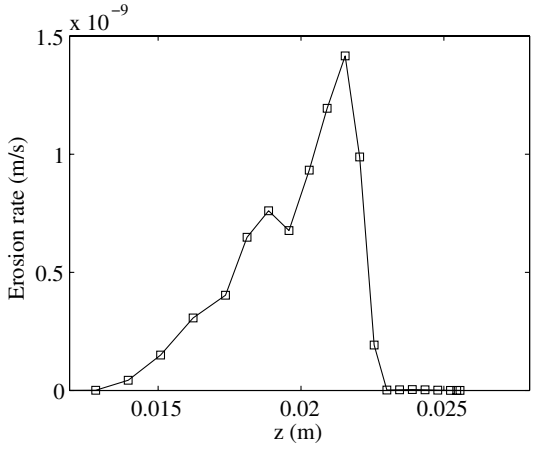

Fig. 21 BHT-200: erosion rate from 400–500 h of operation.

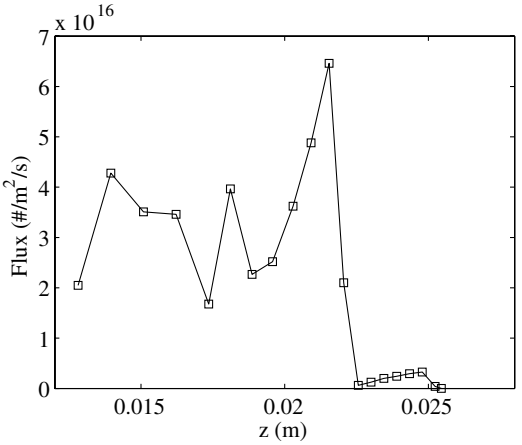

Fig. 22 BHT-200: ion flux from 400–500 h of operation.

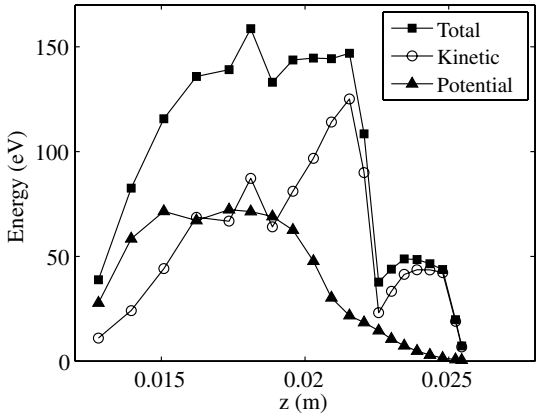

Fig. 23 BHT-200: ion energy from 400–500 h of operation.

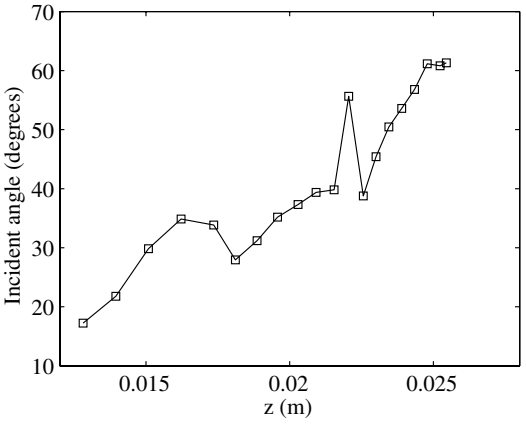

Fig. 24 BHT-200: ion incident angle from 400–500 h of operation.

shortcoming of the simulation can be attributed to a lack of understanding in the sputter yield and anomalous transport models. By adjusting the sputtering model via the sputter threshold and the transport model via the Bohm coefficient and transport barrier position, agreement to either the erosion or the performance can be attained. Though tuning was extensive, it was not exhaustive and it is possible the correct combination of parameters could yield success on both metrics. However, the uncertainty in both fundamental physics models suggests further basic research is needed before progressing with the lifetime issue, which is currently an exercise in educated adjustment of parameters. Along with a deeper theoretical insight into the low-energy sputtering and anomalous transport processes, experimental measurements of sputter yield at low energy and internal discharge plasma parameters are key to the continued development of accurate lifetime prediction models. Although the empirical thruster erosion profiles can serve as an interior diagnostic by dispensing clues about the fluxes and energies of ions flowing to the walls, concrete data such as the potential or plasma density profile along the channel would enable pinning of the computational model to reality.

Further improvements to the current computational model can be envisioned. For example, it is known that small-scale details of a surface affect its erosion. As discussed in Sec. V, the grid size is dictated by the hybrid PIC methodology and precludes capturing surface morphologies smaller than a Debye length. Further, sputtered material from the wall may be redeposited on other thruster surfaces and affect erosion in this manner. Although these issues were

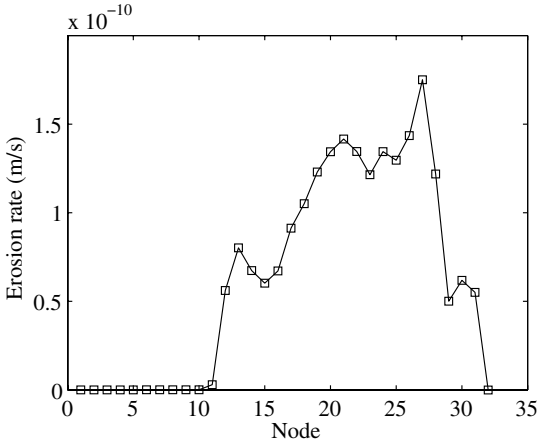

Fig. 25 BHT-600: inner insulator erosion rate from 494 h of operation.

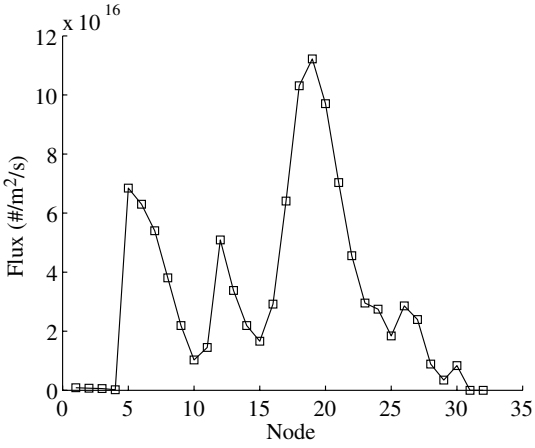

Fig. 26 BHT-600: inner insulator ion flux from 494 h of operation.

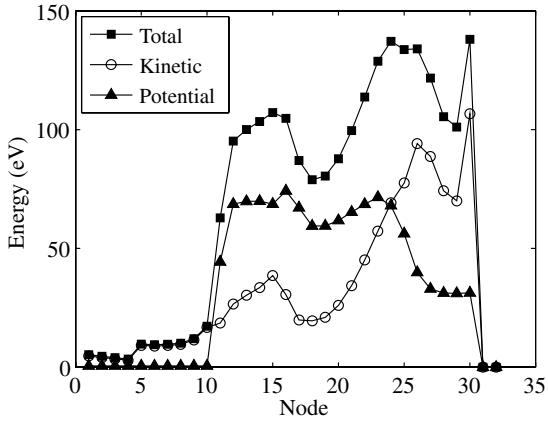

Fig. 27 BHT-600: inner insulator ion energy from 494 h of operation.

considered when developing the erosion model, they were omitted from the final simulation due to lack of reality-based physics models for these processes. Thus, the current model can only provide a general picture of the thruster erosion, which may be sufficient for estimating lifetime or aiding in the design process. Until the current state of knowledge is improved with better understanding of basic physics, it is unrealistic to expect that further advancement in the details of accurately predicting erosion and lifetime will be achieved.

IX. Conclusions

A multiscale Hall thruster model that spans time scales on the order of tens of nanoseconds up to hundreds of hours has been developed to predict the erosion mechanisms that determine the lifetime of the device. The attention paid to definition of thruster geometry and magnetic field has eliminated these parameters as sources of error and allows closer examination of possible discrepancies in the underlying physics models. It is found that greater understanding of the mechanisms affecting near-threshold sputtering and anomalous transport is critical to progressing with the problem. By investigating two thrusters with significantly different geometries, the contrast in the evolution of their erosion profiles points to the problem being thruster-specific. Lifetime prediction models must take these disparities into account, and generic approaches are not adequate.

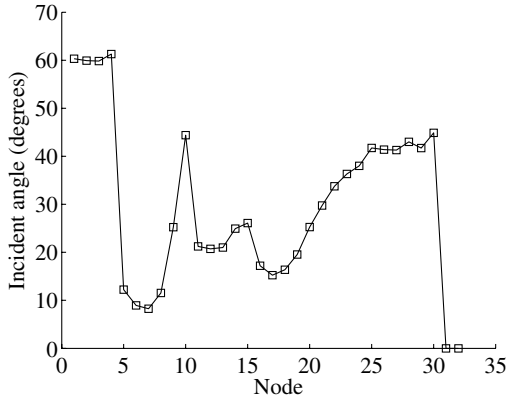

Fig. 28 BHT-600: inner insulator ion incident angle from 494 h of operation.

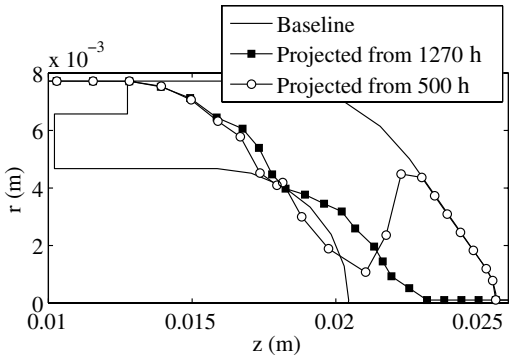

Fig. 29 BHT-200 projected end of life profiles (1330 h).

References

[1] Vinogradov, V. N., Murashko, V. M., and Scortecci, F., "Cost-Optimum Electric Propulsion for Constellations," *Journal of Spacecraft and Rockets*, Vol. 39, No. 1, Jan.–Feb. 2002, pp. 146–149.

[2] Frisbee, R. H., "Evaluation of High-Power Solar Electric Propulsion Using Advanced Ion, Hall, MPD, and PIT Thrusters for Lunar and Mars Cargo Missions," 42nd AIAA/ASME/SAE/ASEE Joint Propulsion Conference and Exhibit, Sacramento, CA, AIAA Paper 2006-4465, July 2006.

[3] Winski, R., Wang, J., Carpenter, C., Cassady, J., and Hoskins, A., "Lunar Robotic Precursor Missions Using Electric Propulsion," 42nd AIAA/ASME/SAE/ASEE Joint Propulsion Conference and Exhibit, Sacramento, CA, AIAA Paper 2006-5165, July 2006.

[4] Hofer, R. R., Randolph, T. M., Oh, D. Y., Snyder, J. S., and deGrys, K. H., "Evaluation of a 4.5 kW Commercial Hall Thruster System for NASA Science Missions," 42nd AIAA/ASME/SAE/ASEE Joint Propulsion Conference and Exhibit, Sacramento, CA, AIAA Paper 2006-4469, July 2006.

[5] Dankanich, J. W., and Polsgrove, T., "Mission Benefits of Gridded Ion and Hall Thruster Hybrid Propulsion Systems," 42nd AIAA/ASME/SAE/ASEE Joint Propulsion Conference and Exhibit, Sacramento, CA, AIAA Paper 2006-5162, July 2006.

[6] Garner, C. E., Brophy, J. R., Polk, J. E., and Pless, L. C., "A 5,730-Hr Cyclic Endurance Test of the SPT-100," 31st AIAA/ASME/SAE/ASEE Joint Propulsion Conference and Exhibit, San Diego, CA, AIAA Paper 1995-2667, July 1995.

[7] Arkhipov, B., Bober, A. S., Gnizdor, R. Y., Kozubsky, K. N., Korakin, A. I., Maslennikov, N. A., and Pridannikov, S. Y., "The Results of 7000-Hour SPT-100 Life Testing," 24th International Electric Propulsion Conference, Moscow, International Electric Propulsion Conference Paper 1995-39, Sept. 1995.

[8] Petrosov, V. A., Vasin, A. I., Baranov, V. I., Wetch, J. R., Britt, E. J., Wong, S. P., and Lin, R., "A 2000 Hours Lifetime Test Results of 1.3 kW T-100 Electric Thruster," 24th International Electric Propulsion Conference, Moscow, International Electric Propulsion Conference Paper 1995-41, Sept. 1995.

[9] Mason, L. S., Jankovsky, R. S., and Manzella, D. H., "1000 Hours of Testing on a 10 Kilowatt Hall Effect Thruster," 37th AIAA/ASME/SAE/ASEE Joint Propulsion Conference and Exhibit, Salt Lake City, UT, AIAA Paper 2001-3773, July 2001.

[10] Marchandise, F. R., Biron, J., Gambon, M., Cornu, N., Darnon, F., and Estublier, D., "The PPS-1350 Qualification Demonstration 7500 h on Ground, About 5000 h in Flight," 29th International Electric Propulsion Conference, Princeton, NJ, International Electric Propulsion Conference Paper 2005-209, Oct. 2005.

[11] de Grys, K., Welander, B., Dimicco, J., Wenzel, S., Kay, B., Khayms, V., and Paisley, J., "4.5 kW Hall Thruster System Qualification Status," 41st AIAA/ASME/SAE/ASEE Joint Propulsion Conference and Exhibit, Tucson, AZ, AIAA Paper 2005-3682, July 2005.

[12] Garner, C. E., Brophy, J. R., Polk, J. E., Semenkin, S., Garkusha, V., Tverdokhlebov, S., and Marrese, C., "Experimental Evaluation of Russian Anode Layer Thrusters," 30th AIAA/ASME/SAE/ASEE Joint Propulsion Conference and Exhibit, Indianapolis, IN, AIAA Paper 1994-3010, June 1994.

[13] Semenkin, A., Kochergin, A., Rusakov, A., Bulaev, V., Yuen, J., Shoji, J., Garner, C., and Manzella, D., "Development Program and Preliminary Test Results of the TAL-110 Thruster," 35th AIAA/ASME/SAE/ASEE Joint Propulsion Conference and Exhibit, Los Angeles, AIAA Paper 1999-2279, June 1999.

[14] Jacobson, D. T., "High Voltage TAL Erosion Characterization," 38th AIAA/ASME/SAE/ASEE Joint Propulsion Conference and Exhibit, Indianapolis, IN, AIAA Paper 2002-4257, July 2002.

[15] Peterson, P. Y., and Manzella, D. H., "Investigation of the Erosion Characteristics of a Laboratory Hall Thruster," 39th AIAA/ASME/SAE/ASEE Joint Propulsion Conference and Exhibit, Huntsville, AL, AIAA Paper 2003-5005, July 2003.

[16] Solodukhin, A. E., and Semenkin, A. V., "Study of Discharge Channel Erosion in Multi Mode Anode Layer Thruster," 28th International Electric Propulsion Conference, Toulouse, France, International Electric Propulsion Conference Paper 2003-0204, March 2003.

[17] Bugrova, A. I., Bishaev, A. M., Desyatskov, A. V., Kozintseva, M. V., and Prioul, M., "Spectral Investigation of SPT MAG Insulator Erosion," 29th International Electric Propulsion Conference, Princeton, NJ, International Electric Propulsion Conference Paper 2005-167, Oct. 2005.

[18] Dyshlyuk, E. N., and Gorshkov, O., "Spectroscopic Investigation of a Hall Thruster Ceramic Acceleration Channel Erosion Rate," 42nd AIAA/ASME/SAE/ASEE Joint Propulsion Conference and Exhibit, Sacramento, CA, AIAA Paper 2006-4660, July 2006.

[19] Tverdokhlebov, O. S., and Karabadzhak, G. F., "TAL Relative Erosion Rate Real-Time Measurements Through Analysis of its Emission Spectra," 28th International Electric Propulsion Conference, Toulouse, France, International Electric Propulsion Conference Paper 2003-0336, March 2003.

[20] Yamamoto, N., Yokota, S., Matsui, M., Komurasaki, K., and Arakawa, Y., "Estimation of Erosion Rate by Absorption Spectroscopy in a Hall Thruster," 29th International Electric Propulsion Conference, Princeton, NJ, International Electric Propulsion Conference Paper 2005-037, Oct. 2005.

[21] Gorshkov, O. A., Shagayda, A. A., and Irishkov, S. V., "The Influence of the Magnetic Field Topology on Hall Thruster Performance," 42nd AIAA/ASME/SAE/ASEE Joint Propulsion Conference and Exhibit, Sacramento, CA, AIAA Paper 2006-4472, July 2006.

[22] Manzella, D., Yim, J., and Boyd, I., "Predicting Hall Thruster Operational Lifetime," 40th AIAA/ASME/SAE/ASEE Joint Propulsion Conference and Exhibit, Fort Lauderdale, FL, AIAA Paper 2004-3953, July 2004.

[23] Yim, J. T., Keidar, M., and Boyd, I. D., "An Evaluation of Sources of Erosion in Hall Thrusters," 41st AIAA/ASME/SAE/ASEE Joint Propulsion Conference and Exhibit, Tucson, AZ, AIAA Paper 2005-3530, July 2005.

[24] Yim, J. T., Keidar, M., and Boyd, I. D., "A Hydrodynamic-Based Erosion Model for Hall Thrusters," 29th International Electric Propulsion Conference, Princeton, NJ, International Electric Propulsion Conference Paper 2005-013, Oct. 2005.

[25] Yim, J. T., Keidar, M., and Boyd, I. D., "An Investigation of Factors Involved in Hall Thruster Wall Erosion Modeling," 42nd AIAA/ASME/SAE/ASEE Joint Propulsion Conference and Exhibit, Sacramento, CA, AIAA Paper 2006-4657, July 2006.

[26] Garrigues, L., Hagelaar, G. J. M., Bareilles, J., Boniface, C., and Bouef. J. P., "Model Study of the Influence of the Magnetic Field Configuration on the Performance and Lifetime of a Hall Thruster," *Physics of Plasmas*, Vol. 10, No. 12, Dec. 2003, pp. 4886–4892. doi:10.1063/1.1622670

[27] Fife, J. M., "Two-Dimensional Hybrid Particle-In-Cell Modeling of Hall Thrusters," S.M. Thesis, Massachusetts Inst. of Technology, Cambridge, MA, May 1995.

[28] Fife, J. M., "Hybrid-PIC Modeling and Electrostatic Probe Survey of Hall Thrusters," Ph.D. Thesis, Dept. of Aeronautics and Astronautics, Massachusetts Inst. of Technology, Cambridge, MA, Sept. 1998.

[29] Gamero-Castaño, M., and Katz, I., "Estimation of Hall Thruster Erosion Using HPHall," 29th International Electric Propulsion Conference, Princeton, NJ, International Electric Propulsion Conference Paper 2005-303, Oct. 2005.

[30] Absalamov, S. K., Andreev, V. B., Colbert, T., Day, M., Egorov, V. V., Gnizdor, R. U., Kaufman, H., Kim, V., Korakin, A., Kozubsky, K. N., Kudravzev, S. S., Lebedev, U. V., Popov, G. A., and Zhurin, V. V., "Measurement of Plasma Parameters in the Stationary Plasma Thruster (SPT-100) Plume and its Effects on Spacecraft Components," 28th AIAA/ASME/SAE/ASEE Joint Propulsion Conference and Exhibit, Nashville, TN, AIAA Paper 1992-3156, July 1992.

[31] Hofer, R. R., Katz, I., Mikellides, I. G., and Gamero-Castaño, M., "Heavy Particle Velocity and Electron Mobility Modeling in Hybrid-PIC Hall Thruster Simulations," 42nd AIAA/ASME/SAE/ASEE Joint Propulsion Conference and Exhibit, Sacramento, CA, AIAA Paper 2006-4658, July 2006.

[32] Hofer, R. R., Mikellides, I. G., Katz, I., and Goebel, D. M., "Wall Sheath and Electron Mobility Modeling in Hybrid-PIC Hall Thruster Simulations," 43rd AIAA/ASME/SAE/ASEE Joint Propulsion Conference and Exhibit, Cincinnati, OH, AIAA Paper 2007-5267, July 2007.

[33] Sommier, E., Allis, M. K., and Cappelli, M. A., "Wall Erosion in 2D Hall Thruster Simulations," 29th International Electric Propulsion Conference, Princeton, NJ, International Electric Propulsion Conference Paper 2005-189, Oct. 2005.

[34] Sommier, E., Allis, M. K., Gascon, N., and Cappelli, M. A., "Wall Erosion in 2D Hall Thruster Simulations," 42nd AIAA/ASME/SAE/ASEE Joint Propulsion Conference and Exhibit, Sacramento, CA, AIAA Paper 2006-4656, July 2006.

[35] Garnier, Y., Roussel, J.-F., and Bernard, J., "Low-energy xenon ion sputtering of ceramics investigated for stationary plasma thrusters," *Journal of Vacuum Science and Technology A (Vacuum, Surfaces, and Films)*, Vol. 17, No. 6, Nov.–Dec. 1999, pp. 3246–3254. doi:10.1116/1.582050

[36] Yalin, A. P., Surla, V., Farnell, C., Butweiller, M., and Williams, J. D., "Sputtering Studies of Multi-Component Materials by Weight Loss and Cavity Ring-Down Spectroscopy," 42nd AIAA/ASME/SAE/ASEE Joint Propulsion Conference and Exhibit, Sacramento, CA, AIAA Paper 2006-4338, July 2006.

[37] Yamamura, Y., and Tawara, H., "Energy Dependence of Ion-Induced Sputtering Yields from Monatomic Solids at Normal Incidence," *Atomic Data and Nuclear Data Tables*, Vol. 62, No. 2, March 1996, pp. 149–253. doi:10.1006/adnd.1996.0005

[38] Yamamura, Y., "An Empirical Formula for Angular Dependence of Sputtering Yields," *Radiation Effects and Defects in Solids*, Vol. 80, Nos. 1–2, Feb. 1984, pp. 57–72. doi:10.1080/00337578408222489

[39] Parra, F. I., Ahedo, E., Fife, J. M., and Martinez-Sanchez, M., "A Two-Dimensional Hybrid Model of the Hall Thruster Discharge," *Journal of Applied Physics*, Vol. 100, No. 2, July 2006, Paper 023304. doi:10.1063/1.2219165

[40] Cappelli, M. A., Meezan, N. B., and Gascon, N., "Transport Physics in Hall Plasma Thrusters," 40th AIAA Aerospace Sciences Meeting and Exhibit, Reno, NV, AIAA Paper 2002-0485, Jan. 2002.

[41] Allis, M. K., Thomas, C. A., Gascon, N., Cappelli, M. A., and Fernandez, E., "Introduction of Physical Transport Mechanisms into 2D Hybrid Hall Thruster Simulations," 42nd AIAA/ASME/SAE/ASEE Joint Propulsion Conference and Exhibit, Sacramento, CA, AIAA Paper 2006-4325, July 2006.

[42] Fox, J. M., Batishcheva, A. A., Batishchev, O. V., and Martinez-Sanchez, M., "Adaptively Meshed Fully-Kinetic PIC-Vlasov Model For Near Vacuum Hall Thrusters," 42nd AIAA/ASME/SAE/ASEE Joint Propulsion Conference and Exhibit, Sacramento, CA, AIAA Paper 2006-4324, July 2006.

[43] Allis, M. K., Gascon, N., Vialard-Goudou, C., Cappelli, M. A., and Fernandez, E., "A Comparison of 2-D Hybrid Hall Thruster Model to Experimental Measurements," 40th AIAA/ASME/SAE/ASEE Joint Propulsion Conference and Exhibit, Fort Lauderdale, FL, AIAA Paper 2004-3951, July 2004.

[44] Fox, J. M., "Parallelization of a Particle-in-Cell Simulation Modeling Hall-Effect Thrusters," M.S. Thesis, Massachusetts Inst. of Technology, Cambridge, MA, Jan. 2005.

[45] Koo, J. W., and Boyd, I. D., "Anomalous Electron Mobility Modeling in Hall Thrusters," 41st AIAA/ASME/SAE/ASEE Joint Propulsion Conference and Exhibit, Tucson, AZ, AIAA Paper 2005-4057, July 2005.

[46] "Hall Effect Thruster Systems," May 2007, http://www.busek.com/halleffect.html.

[47] Cheng, S. Y., "Modeling of Hall Thruster lifetime and Erosion Mechanisms," Ph.D. Thesis, Dept. of Aeronautics and Astronautics, Massachusetts Inst. of Technology, Cambridge, MA, May 2007.

A. Gallimore
Associate Editor